

# Co(OH)<sub>2</sub> hollow nanoflowers as highly efficient electrocatalysts for oxygen evolution reaction

Hongfei Liu,<sup>c)</sup> Dingyi Guo,<sup>c)</sup> and Wei Zhang<sup>a)</sup>

*School of Chemistry and Chemical Engineering, Shaanxi Normal University, Xi'an 710119, China*

Rui Cao<sup>b)</sup>

*School of Chemistry and Chemical Engineering, Shaanxi Normal University, Xi'an 710119, China; and Department of Chemistry, Renmin University of China, Beijing 100872, China*

(Received 29 July 2017; accepted 5 September 2017)

Electrocatalytic water splitting for the production of H<sub>2</sub> is increasingly becoming a significant method to mitigate the current energy crisis and environmental pollution. However, oxygen evolution reaction (OER), a slow four-electron process, is the bottle neck of water splitting. Thus, developing new, low cost, and effective catalysts for OER is a research hotspot in material and energy resource fields. Therefore, the research of nonprecious, metal-based OER catalysts has been popular. In this work, it is validated that 3D hollow Co(OH)<sub>2</sub> nanoflowers synthesized by a facile template-based strategy at room temperature are effective electrocatalysts for OER. The catalysts display high activity with a current density of 10 mA/cm<sup>2</sup> at an overpotential of 310 mV and a small Tafel slope of 68.9 mV/dec in alkaline condition. It's noteworthy that this material is stable for over 20 h of chronopotentiometry. This work offers a simple and promising way to prepare efficient and durable electrocatalysts.

## I. INTRODUCTION

Everyone is responsible for handling the present and future fuel feed and related environmental issues in the 21st century. Chemists are considered in duty bound and competent to overcome corresponding technological challenges. As is well known, carbon-based and non-renewable fossil fuels, including coal, crude oil, and natural gas, still dominate the whole world energy supply nowadays. As a result, the huge consumption of limited fossil fuels will cause energy depletion and bring about serious environmental contamination and climate change, which threatens human health, ecological sustainability, and social progress. Thus, we should cut the use of fossil fuels and exploit new energy, which must be abundant, low cost, pollution free and inexhaustible. To satisfy these requirements, sunlight may be the optimal choice. Photosynthesis is widespread in nature. During this process, chlorophyll collects solar energy to convert water and carbon dioxide into organic compounds and release oxygen. In a word, sunlight energy is converted into chemical energy through photosynthesis and the obtained chemical energy is stored for valuable uses. In detail, the chemical reaction starts with the photoreaction

converting water into free protons and electrons and liberating oxygen. Inspired by the scenery of fuel generation powered by solar energy, scientists have paid close attention to the research field of artificial photosynthesis. However, artificial photosynthesis is difficult to achieve due to the lack of an effective catalyst. In recent years, artificial photosynthesis has drawn public attention to handle the environmental pollution and energy crisis due to the excessive use of traditional fossil fuels.<sup>1–6</sup> Hydrogen, a sustainable, clean, eco friendly, and economic energy with a superior gravimetric energy density, is known as a potential candidate for new energy resources.<sup>7–13</sup> It is mentionable that the sole combustion exhaust of hydrogen is pollution-free water. Moreover, clear molecular hydrogen can be obtained from abundant water resource easily. The whole process shows a perfect circulation without any pollutant discharged, which is completely in conformity with the new energy resource standard. Water splitting, including hydrogen evolution reaction and oxygen evolution reaction (OER), is an attractive way to generate hydrogen efficiently.<sup>14–21</sup> However, OER is the bottleneck in the whole water splitting process because it's a multistep proton-coupled electron transfer (PCET) process. PCET plays significant roles in many chemical and biological reactions related to energy conversion. The relationship between PCET and the energy conversion reaction has been studied in a review from Meyer and coworkers, in which many underlying principles about PCET have been summarized.<sup>22</sup> PCET plays a crucial part during OER

Contributing Editor: Yao Zheng

Address all correspondence to these authors.

<sup>a)</sup>e-mail: zw@snnu.edu.cn

<sup>b)</sup>e-mail: ruicao@ruc.edu.cn

<sup>c)</sup>These authors contributed equally to this work.

DOI: 10.1557/jmr.2017.390

whether thermodynamically or kinetically. In thermodynamics, PCET can effectively avert the charge build up effect and successfully accelerate catalyst activation. In dynamics, PCET can avoid the formation of high-energy intermediates through the simultaneous transfer of electrons and protons to a degree. It is hard to accomplish OER due to the high-energy barrier and slow-reaction dynamics.<sup>23–26</sup> In detail, two water molecules are required to take part in the oxidation reaction to produce one oxygen molecule during the OER process according to the law of the conservation of mass. At the same time, two proton-electron couples must leave from each water molecule to meet the requirement of charge conservation. In other words, generating an oxygen molecule requires four proton-electron couples lost from two water molecules in total, which is an intricate process. In other words, the process of O–H bond breaking and attendant O–O bond formation is difficult. Thus, the researchers worldwide are searching for highly active catalysts to accelerate the reaction and reduce the overpotential of OER. Generally, an excellent OER catalyst should meet three essential criterions. First, high activity with considerable current density is required at low overpotentials. Second, superior durability in mild conditions is also a requisite. OER catalysts with both high activity and superior durability can be meaningful and used for large-scale applications. Third, simple and safe synthetic method is also needed. To our knowledge, the most effective catalysts for water oxidation in both acidic and alkaline conditions are noble metal-based RuO<sub>2</sub> and IrO<sub>2</sub>.<sup>27</sup> However, the low abundance and high cost largely hinder their large-scale applications. Thus, it is still a challenge to develop inexpensive, easily accessible, highly efficient, and stable catalysts as alternative candidates.

Many efficient OER catalysts with nonprecious metal elements have been reported.<sup>28</sup> Among the various catalysts, the first-row transition metal-based (Mn, Fe, Co, Ni, and Cu etc.) materials including their oxides,<sup>29–39</sup> (oxy)hydroxides,<sup>40–45</sup> layered double hydroxides,<sup>46–51</sup> sulfides,<sup>52–55</sup> selenides,<sup>56–61</sup> borides,<sup>62,63</sup> carbides,<sup>64</sup> nitrides,<sup>65,66</sup> and phosphate<sup>67–76</sup> have been extensively studied as highly efficient OER catalysts. Cobalt is considered as an attractive nonnoble metal for its better catalytic ability toward OER with many merits, such as abundant reserves, nonpoisonous, various valences, and good electrical conductivity. Extensive study efforts have been devoted to proving that Co-based homogenous molecular catalysts are widely considered as promising candidates for OER.<sup>77,78</sup> However, the actual application of these homogenous catalysts is often limited by their weak durability, inferior activity, and large overpotential. Additionally, homogenous molecular OER catalysts should be equipped with excellent water solubility, which is difficult during the design and synthesis of the

molecules. Therefore, considerable current investigations have been focused on exploiting Co-based inorganic materials as heterogeneous OER catalysts possessing excellent OER activity and super stability. Especially, Co-based nanometer materials with small sizes are popular. Recently, we and other groups have studied a number of Co-based materials exhibiting prominent OER performance with innovative morphologies.<sup>79–82</sup> Noteworthy, the three-dimensional Co(OH)F microspheres, which are structured by low-dimensional building units step by step, have shown a promising OER performance. Particularly,  $\alpha$ -Co(OH)<sub>2</sub> owns good electrical conductivity, unique layered structure, and larger surface area, which is beneficial for electrocatalytic reaction. Furthermore, it is inexpensive and eco friendly. Thus,  $\alpha$ -Co(OH)<sub>2</sub> catches the attention of researchers as a potential electrode material, especially in the application of supercapacitors.<sup>83,84</sup> However, there has been much less investigation on  $\alpha$ -Co(OH)<sub>2</sub> as water oxidation catalysts.<sup>85,86</sup> On the other hand, the morphologies and phases of nanomaterials play a vital role in their properties and applications. In particular, three-dimensional (3D) flower-like nanostructures possessing relatively open spaces may be beneficial for the rapid electron transfer process and fast diffusion of ions toward the outstanding electrocatalytic activity. Till today, synthetic methods of flower-like architecture still need to be improved due to long time, high-cost, and poor efficiency of the present means. Additionally, the amorphous  $\alpha$ -Co(OH)<sub>2</sub> can offer more catalytic active sites due to the unordered structure, which open the door to employ amorphous  $\alpha$ -Co(OH)<sub>2</sub> as the superior OER catalyst. In general, Co(OH)<sub>2</sub> was fabricated by hydro/solvo-thermal methods. It usually requires a relatively high temperature and a long time for the costly synthesis. Normally, amorphous Co(OH)<sub>2</sub> was obtained through the electrochemistry techniques, which are invalid for large-scale commercial applications due to expensive production costs. To address these limitations, we adopted a facile template-based route to synthesize 3D  $\alpha$ -Co(OH)<sub>2</sub> hollow nanoflowers comprising of ultrathin nanoflakes at room temperature in this work. Furthermore, the 3D  $\alpha$ -Co(OH)<sub>2</sub> material is amorphous in this work, which is pivotal to the whole OER process. It has been reported that amorphous Co(OH)<sub>2</sub> nanostructures possess superior OER activity than that of the corresponding crystalline materials.<sup>87</sup> We are encouraged by such research results to search for simple and reliable methods of generating amorphous Co(OH)<sub>2</sub> nanometer materials for OER. In detail, Cu<sub>2</sub>O nanospheres, the sacrificial templates, were synthesized via a previously reported method with little modification. Then,  $\alpha$ -Co(OH)<sub>2</sub> hollow nanoflowers (denoted as  $\alpha$ -Co(OH)<sub>2</sub>/HNFs) were fabricated in a Na<sub>2</sub>S<sub>2</sub>O<sub>3</sub> solution. During this process, Na<sub>2</sub>S<sub>2</sub>O<sub>3</sub> plays two significant roles. It was first used as a coordinating

ligand to interact with Cu<sub>2</sub>O, and it is incapable of reacting with Co<sup>2+</sup>, which is forecasted by classical hard and soft acids and bases principle. Second, S<sub>2</sub>O<sub>3</sub><sup>2-</sup> can hydrolyze to generate OH<sup>-</sup>, which will combine with the dissociative Co<sup>2+</sup> to lead to the precipitation of α-Co(OH)<sub>2</sub> on the surface of the Cu<sub>2</sub>O template. Noteworthy, no other etching agents were used to remove the Cu<sub>2</sub>O template, which is superior to the traditional methods of templated synthesis. In our work, the alkali source S<sub>2</sub>O<sub>3</sub><sup>2-</sup> is considered as the etching agent at the same time, which can avoid the introduction of impurity effectively. Both of above characteristics facilitate the fabrication of α-Co(OH)<sub>2</sub>/HNFs. The as-prepared Co(OH)<sub>2</sub> exhibited high activity for electrocatalytic water oxidation and is better than α-Co(OH)<sub>2</sub> and β-Co(OH)<sub>2</sub> nanoplates. In addition, the resulting catalyst demonstrated excellent stability for 20 h. This facile template-based strategy to synthesize amorphous metal hydroxides or oxides has potential in electrocatalytic areas. We also synthesized α-Co(OH)<sub>2</sub> nanosheets [denoted as α-Co(OH)<sub>2</sub>/NSs] and β-Co(OH)<sub>2</sub> nanosheets [denoted as β-Co(OH)<sub>2</sub>/NSs] as contrast samples.

## II. MATERIALS AND METHODS

### A. General materials

All chemicals, including copper(II) acetate monohydrate (99%, Energy Chemical, Shanghai, China), polyvinylpyrrolidone (PVP; average Mw 40,000, Energy Chemical, Shanghai, China), polyvinylpyrrolidone (average Mw 24,000, Xiya Reagent, Shandong, China), hexamethylenetetramine (99.5%, Energy Chemical, Shanghai, China), sodium borohydride (98%, Energy Chemical, Shanghai, China), cobalt chloride hexahydrate (95%, Heowns Biochem LLC, Tianjin, China), sodium thiosulfate pentahydrate (98%, Sinopharm Chemicals, Shanghai, China), potassium hydroxide (98%, Sinopharm Chemicals), absolute ethanol (Sinopharm Chemicals, Shanghai, China), and *N,N*-dimethylformamide (DMF; 99%, Sinopharm Chemicals, Shanghai, China) were obtained from commercial suppliers and used without further purification unless otherwise noted. Milli-Q water of 18 MΩ cm was used in all experiments.

### B. Synthesis of Cu<sub>2</sub>O nanospheres

The Cu<sub>2</sub>O nanospheres were synthesized by the method reported in the literature with little modification.<sup>88</sup> In this reaction, NaBH<sub>4</sub> is used as a strong reductive agent to react with Cu(CH<sub>3</sub>COO)<sub>2</sub>·H<sub>2</sub>O for producing the Cu<sub>2</sub>O precipitate, which was completed with the help of a trace amount of H<sub>2</sub>O from DMF. DMF is considered as the reaction solvent with an inferior reaction temperature. PVP is introduced to regulate and control the morphology of Cu<sub>2</sub>O nanospheres. In a typical experiment, 0.8 g Cu(CH<sub>3</sub>COO)<sub>2</sub>·H<sub>2</sub>O and 0.1 g PVP

(MW: 40,000) were dispersed in 40 mL DMF by stirring for 10 min. 75.6 mg NaBH<sub>4</sub> was added under stirring for another 10 min. Then, the above mixture was heated to 90 °C until the color changed from brownish black to earthy yellow. Finally, the mixture was cooled to room temperature and collected by centrifugation, washed with deionized water and absolute ethanol separately for three times, and dried at 60 °C for overnight.

### C. Synthesis of Co(OH)<sub>2</sub>/HNFs

Co(OH)<sub>2</sub> hollow nanoflowers were prepared by a simple method at room temperature.<sup>89</sup> In a typical procedure, 20 mg Cu<sub>2</sub>O was uniformly dispersed in 10 mL H<sub>2</sub>O and 10 mL ethanol-mixed solutions. After stirring for 5 min at room temperature, 600 mg PVP (MW: 24,000) was added. The solution was stirred for another 10 min, then, 0.5 mL CoCl<sub>2</sub>·6H<sub>2</sub>O (26 mg) solution was added as the cobalt source. After that, 2 mL of 2 M Na<sub>2</sub>S<sub>2</sub>O<sub>3</sub> solution was added dropwise as both the alkali source and etching agent. At last, the solution was stirred for 5 min. The color of the above mixture was gradually changing from orange red to light green. As a matter of fact, orange Cu<sub>2</sub>O templates faded away and light green Co(OH)<sub>2</sub> gradually generated. The experimental phenomenon manifests that complete etching of the inner Cu<sub>2</sub>O templates and successful synthesis of Co(OH)<sub>2</sub> with a short reaction time required. Finally, the products were collected through certification and then washed with deionized water and absolute ethanol for three times at least and then dried at 60 °C for overnight.

### D. Synthesis of α-Co(OH)<sub>2</sub>/NSs

α-Co(OH)<sub>2</sub> nanosheets were synthesized as a contrast sample. In a typical procedure, 237.9 mg CoCl<sub>2</sub>·6H<sub>2</sub>O and 70.1 mg C<sub>6</sub>H<sub>12</sub>N<sub>4</sub> were dispersed in 20 mL deionized water with magnetic stirring for 5 min. The above solution was transferred into a 50 mL of Teflon-lined autoclave and then kept at 90 °C for 5 h. The collected precipitate was washed with deionized water and dried at 60 °C for overnight.

### E. Synthesis of β-Co(OH)<sub>2</sub>/NSs

β-Co(OH)<sub>2</sub> nanosheets were synthesized as a contrast sample. Briefly, 237.9 mg CoCl<sub>2</sub>·6H<sub>2</sub>O was dissolved in 20 mL deionized water and then 2 mL 2 M NaOH solution was gradually added. The above mixture was continuously stirred for 10 min. Finally, the precipitate was collected by centrifugation, washed with deionized water, and dried at 60 °C overnight.

### F. Preparation of electrode

The working electrode was prepared by a drop-casting method as the following procedure. Typically, 4 mg of the corresponding catalyst was dispersed into 1 mL of water-ethanol solution (which was prepared by mixing H<sub>2</sub>O and

ethanol at a volume ratio of 2:1) with 30  $\mu\text{L}$  of Nafion solution (5 wt%, DuPont) added. Then, the obtained mixture was sonicated for 30 min to form a homogeneous ink dispersion. Subsequently, 5  $\mu\text{L}$  of the ink was drop-casted equably onto the polished GC (0.07  $\text{cm}^2$ ) electrode, which was dried naturally.

### G. Materials characterization

X-ray diffraction (XRD) patterns were acquired with the 2 $\theta$  range from 5 to 80° on a Bruker D8 Discover X-ray diffractometer (Bruker, Billerica, Massachusetts) with Cu K $\alpha$  radiation ( $\lambda = 1.5406 \text{ \AA}$ ). The morphology and microstructure of the samples were investigated by a field emission scanning electron microscope (FESEM, SU8020, Hitachi, Tokyo, Japan) at an accelerating voltage of 10 kV. The transmission electron microscopy (TEM) images were determined by a TEM (JEM-2100, JEOL Ltd., Beijing, China) with an accelerating voltage of 200 kV. Energy dispersive X-ray (EDX) analysis was carried out on an AMETEK Materials Analysis (Ametek, Shanghai, China). The X-ray photoelectron spectroscopy (XPS) was performed on a Kratos AXIS ULTRA XPS analyzer (Kratos Analytical Ltd., Hadano, Japan) with

monochromatized Al K $\alpha$  ( $h\nu = 1486.6 \text{ eV}$ ) X-ray source. The XPS binding energies were corrected using the C 1s peak at 284.6 eV.

### H. Electrocatalytic measurements

All the electrochemical measurements were performed on the CHI 660E electrochemical workstation equipped with a traditional three-electrode system at room temperature using glass carbon (GC, 0.07  $\text{cm}^2$ ) as the working electrode if not specified, Pt wire as a counter electrode and saturated Ag/AgCl (KCl solution) as the reference electrode. Cyclic voltammograms (CVs) were measured in 1 M KOH solution at a rate of 50 mV/s with iR-compensation. In these measurements, the working electrode was cycled several times to get a steady response before data recording. All the potentials in this article were calibrated to the reversible hydrogen electrode (RHE) according to the equation:  $E_{\text{RHE}} = E_{\text{Ag/AgCl}} + (0.197 + 0.059 \text{ pH}) \text{ V}$ . The electrochemically active surface area (ECSA) was obtained by CV at a non-Faradaic potential window from 1.18 to 1.28 V versus RHE at different scan rates: 20, 40, 60, 80, 100, and 120 mV/s. The charging current densities at the middle potential were plotted versus the scan rate, giving a linear

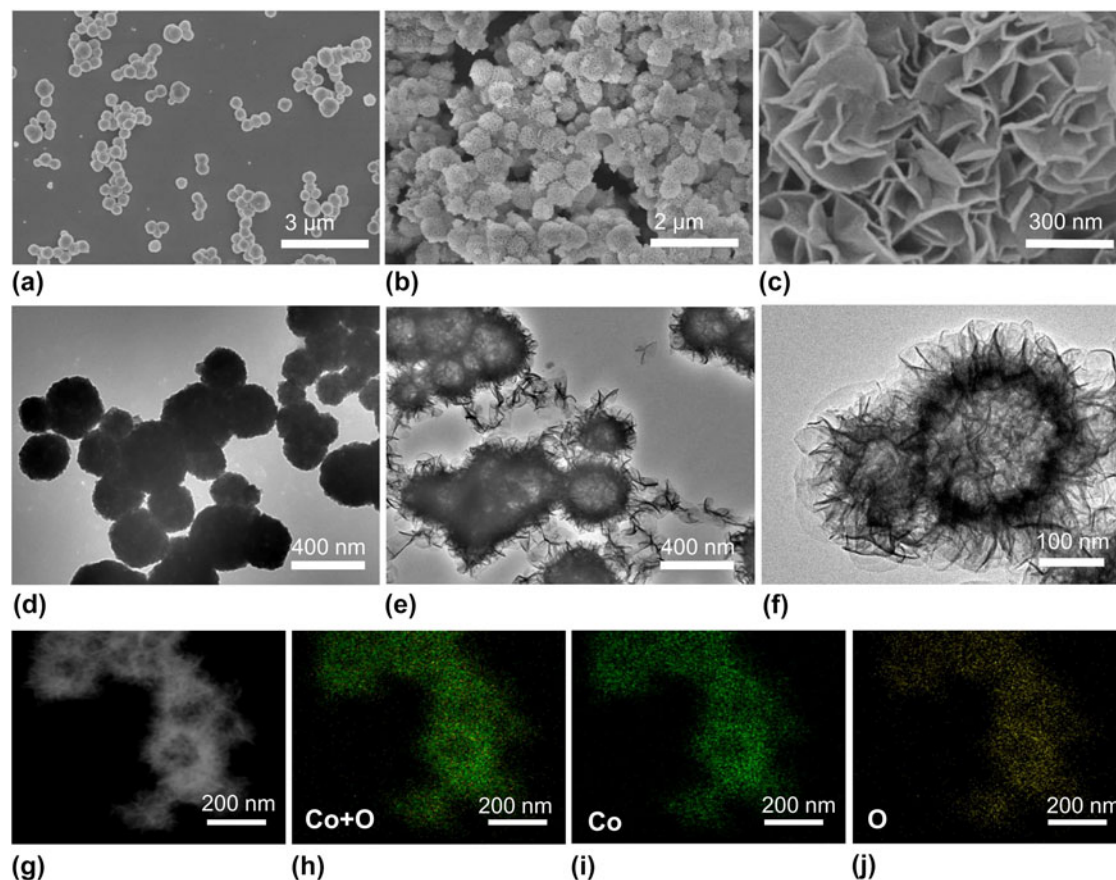


FIG. 1. SEM images of the as-prepared Cu<sub>2</sub>O templates (a) and  $\alpha$ -Co(OH)<sub>2</sub>/HNFs (b, c); TEM images of Cu<sub>2</sub>O (d) and  $\alpha$ -Co(OH)<sub>2</sub>/HNFs (e, f); STEM image (g) and the corresponding elemental mappings (h–j) of the  $\alpha$ -Co(OH)<sub>2</sub>/HNFs.

plot whose slope identified the double-layer capacitance. The electrochemical impedance spectroscopy (EIS) was acquired at 1.65 V versus RHE over a frequency range from 10<sup>6</sup> to 0.1 Hz, with 5 mV as the amplitude potential. Tafel plots were obtained by linear sweep voltammetry tests. Chronopotentiometry and chronoamperometry were carried out in a 1 M KOH aqueous solution to test the stability without iR-compensation with indium-tin oxide (ITO) working electrodes.

### III. RESULTS AND DISCUSSION

#### A. Morphology and structure

The morphologies of as-prepared Cu<sub>2</sub>O templates and  $\alpha$ -Co(OH)<sub>2</sub> were investigated by SEM and TEM. Cu<sub>2</sub>O shows a uniform nanosphere architecture with a diameter of about 300 nm with the assistance of PVP [Figs. 1(a) and 1(d)]. The as-obtained  $\alpha$ -Co(OH)<sub>2</sub> has a three-dimensional nanoflower structure with uniform surface nanoflakes as shown in Figs. 1(b) and 1(c). The thickness of the ultrathin flakes is approximately 10 nm, and the ultrathin flakes stand vertically on the surface to offer open spaces. The numerous surface nanoflakes with a 3D architecture will expose abundant surface active sites, which are favorable for the catalytic process. Further, structure information can be obtained from TEM characterization. TEM images [Figs. 1(e) and 1(f)] indicate that the structure of  $\alpha$ -Co(OH)<sub>2</sub> is hollow and flower-like. By comparing the crust with hollow, the internal cavity leaps to our eyes through the TEM images. A representative image was displayed in Fig. 1(f), in which the transparent areas are in sharp contrast to the dark areas. The formation of dark areas or stripy lines is due to wrinkling, overlapping, or winding of the surface nanoflakes. Therefore, the thickness of the stripy lines identifies the nanoflake thickness. The nearly lucid electron beam in some places can be representative of the unilaminar nanoflake. Such an experimental result testified the thin characteristic of the surface nanoflakes, which will expose more active sites. It should be emphasized that the hollow structural feature and porous shell of  $\alpha$ -Co(OH)<sub>2</sub> may create a superior specific surface area, which leads to a large exchange in current density. Generally, hollow architectures show outstanding electrochemical performance, owing to clear-cut interior cavities and the pivotal shell architecture that can accelerate mass transfer and enhance the electrocatalytic activity.<sup>90</sup> And hollow architectures are also connected with large specific surface area. Moreover, the surface of the hollow nanoflower was rough due to the vertical nanoflake, which causes more active sites exposed than those of the smooth-faced hollow structure. Thus, the special hollow structure of  $\alpha$ -Co(OH)<sub>2</sub> hollow nanoflowers is responsible for their high OER activity. For comparison, SEM images of  $\alpha$ -Co(OH)<sub>2</sub>/NSs and  $\beta$ -Co(OH)<sub>2</sub>/NSs were displayed in Fig. S1.  $\alpha$ -Co(OH)<sub>2</sub>/NSs has an

accumulative nanosheet architecture and  $\beta$ -Co(OH)<sub>2</sub>/NSs shows the hexagonal nanoplate morphology. The average thickness of the nanoplates is determined to be 30 and 40 nm, respectively. In addition, the scanning transmission electron microscopy (STEM) and EDX element mapping were carried out to determine the hollow structure and element distribution of  $\alpha$ -Co(OH)<sub>2</sub>/HNFs. Figures 1(g)–1(j) display the highly uniform dispersion of Co and O in  $\alpha$ -Co(OH)<sub>2</sub>/HNFs and further emphasize the hollow structure with a weak electronic signal of Co and O in the inner cavity.

The unique structure of the  $\alpha$ -Co(OH)<sub>2</sub> hollow flower-like is derived from the elaborate design and synthesis. This work adopted a simple templated synthesis of  $\alpha$ -Co(OH)<sub>2</sub>/HNFs using the uniform Cu<sub>2</sub>O nanosphere as the sacrificial template. Surfactant PVP is significant to assist the formation of high-quality  $\alpha$ -Co(OH)<sub>2</sub>/HNFs. On the one hand, PVP maintain the sphere structure of Cu<sub>2</sub>O by surface interaction. On the other hand, PVP controls the speed of the etching reaction through restricting the movement of S<sub>2</sub>O<sub>3</sub><sup>2-</sup>. The Cu<sub>2</sub>O nanosphere is introduced as sacrificial templates due to the following several advantages. In the first place, essential properties of spherical Cu<sub>2</sub>O can be easily adjusted through argument changes including size, crystallinity, and surface construction. Then, spherical Cu<sub>2</sub>O is synthesized by a simpler method than traditional spherical templates such as silica, carbon colloids, and polymer colloids. Generally, the above-mentioned conventional spherical templates are more difficult for either synthesis preparation or removal. The last but most important is that the Cu<sub>2</sub>O spherical template is favorable to generate the desired  $\alpha$ -Co(OH)<sub>2</sub>/HNFs based on the hard and soft acids and bases principle. Na<sub>2</sub>S<sub>2</sub>O<sub>3</sub> is introduced as the alkali source for generating hydroxide ions and as the coordinating reactant for the removal of Cu<sub>2</sub>O at the same time. Noteworthy, the choice of alkali source in our work is well founded. First, a strong base is impracticable as the alkali source in this work because Co<sup>2+</sup> will precipitate quickly due to the abundant hydroxyl ions resulting from strong bases. As a result, irregular Co(OH)<sub>2</sub> precipitation will be obtained instead of the perfect hollow structure. Na<sub>2</sub>S<sub>2</sub>O<sub>3</sub> can offer moderate alkaline environment for this reaction system, which is favorable for the formation of a hollow structure. Then, hard and soft acids and bases principle offer the theoretical basis for this work. According to this principle, Lewis bases prefer to combine with Lewis acids of the same kind and vice versa. Therefore, hard acids tend to exert better affinity for hard bases but interact unwillingly or infirmly with soft bases. On the other hand, soft acids are more likely to react with soft acids. In other words, a soft-hard combine is impracticable in theory. In this system, the Cu<sup>+</sup> of Cu<sub>2</sub>O template is a soft acid and Co<sup>2+</sup> is a hard acid, so a soft base is more suitable and capable than a hard base

to coordinate with Cu<sup>+</sup> instead of Co<sup>2+</sup>. Thus, a soft base S<sub>2</sub>O<sub>3</sub><sup>2-</sup> was introduced in this work. The whole removal of the template and formation processes of α-Co(OH)<sub>2</sub>/HNFs take place as the following procedure. First, surfactant PVP was used to passivate the surface of Cu<sub>2</sub>O particles and stabilize the shape by PVP adsorption on the surface of the Cu<sub>2</sub>O sphere, which is significant for the morphology control of precipitated α-Co(OH)<sub>2</sub>/HNFs subsequently. Second, two separate reactions take place. On the one hand, soft-base S<sub>2</sub>O<sub>3</sub><sup>2-</sup> combines with soft-acid Cu<sup>+</sup> to accomplish etching of the Cu<sub>2</sub>O template with the soluble complex formed. At the same time, hydroxide ion releases due to the etching of Cu<sub>2</sub>O, and the hydrolysis of S<sub>2</sub>O<sub>3</sub><sup>2-</sup> also makes a contribution to the generation of the hydroxide ion. On the other hand, Co(OH)<sub>2</sub> is formed on the surface of Cu<sub>2</sub>O due to the high concentration of the hydroxide ion close to Cu<sub>2</sub>O. These two reactions occur at the same time, and both take place on the surface of Cu<sub>2</sub>O. Thus, the obtained Co(OH)<sub>2</sub> precipitate inherits the morphology of the Cu<sub>2</sub>O templates. Simultaneously, an inner hollow structure is realized. It must be stated that the size of α-Co(OH)<sub>2</sub>/HNFs in thickness will grow with the above-mentioned reactions. But if the number of Co<sup>2+</sup> reduces to a vital value that is insufficient to satisfy the demand of precipitation, the thickness of the α-Co(OH)<sub>2</sub>/HNFs will no longer increase. At the same time, unbroken corrosion of Cu<sub>2</sub>O can take place even in closed shells, which results in a perfect hollow architecture. In brief, the superior relationship of soft–soft bonding between the etching agent and the template maintains even with a low temperature, which guides the formation of α-Co(OH)<sub>2</sub>/HNFs step by step. As we all know, the conventional template-removal methods always require the introduction of a special etching agent, such as oxidative, reductive, and acidic agents. In our system, S<sub>2</sub>O<sub>3</sub><sup>2-</sup> is considered as the only etching agent and plays other crucial roles at the same time. For example, the formation of the Co(OH)<sub>2</sub> precipitate can be accelerated by the hydroxide ion in high concentration, which results from the hydrolysis of S<sub>2</sub>O<sub>3</sub><sup>2-</sup> and etching of the template.

In a word, the whole material synthesis is based on the classical theoretical basis and presents numerous advantages. The choice of the reaction solvent is also of great importance for the formation of a perfect α-Co(OH)<sub>2</sub> hollow nanosphere. In our system, we choose a water–ethanol solution (which was prepared by mixing H<sub>2</sub>O and ethanol at volume ratio of 1:1) as the optimal reaction solvent. As mentioned above, the whole formation process of α-Co(OH)<sub>2</sub>/HNFs includes two essential reactions: removal of the template and precipitation of α-Co(OH)<sub>2</sub>. If we select water as the only reaction solvent, the hydrolysis of S<sub>2</sub>O<sub>3</sub><sup>2-</sup> will be accelerated without a doubt. As a result, the whole reaction solution shows a high concentration of hydroxide ion. Thus, dissociative Co<sup>2+</sup>

has more chances to react with the hydroxide ion far away from the surface of the template, which leads to the formation of distorted α-Co(OH)<sub>2</sub> spheres or other irregular particles. What is worse is that the sphere architecture will collapse due to the quick mass transfer. At the same time, the concentration of S<sub>2</sub>O<sub>3</sub><sup>2-</sup> will reduce due to the vast hydrolysis, which slows down the reaction speed of template removal with more reaction times. With these factors considered, a certain amount of ethanol is used to limit the hydrolysis of S<sub>2</sub>O<sub>3</sub><sup>2-</sup>. But too much ethanol will not work due to the low ion strength. Of course, the concentration of S<sub>2</sub>O<sub>3</sub><sup>2-</sup> also plays an important role for the formation of α-Co(OH)<sub>2</sub>/HNFs.

In addition to the morphology and structure observation, the phase analysis of resulting samples was determined by XRD. Figure 2(a) shows the XRD pattern of Cu<sub>2</sub>O templates with the characteristic diffraction peaks at 29.6°, 36.5°, 42.4°, 61.5°, 73.7°, and 77.6°, which can be well indexed to the (110), (111), (200), (220), (311), and (222) facets (JCPDS: 75-1531), and no other impure signal can be detected. Figure 2(b) demonstrates that the as-synthesized α-Co(OH)<sub>2</sub>/HNFs sample has four peaks at 9.07°, 19.81°, 33.27°, and 59.44°, which are indexed to the (003), (006), (100), (110) planes.<sup>85</sup> The absence of other peaks indicates a pure phase of α-Co(OH)<sub>2</sub> and a complete removal of the Cu<sub>2</sub>O template. Furthermore, the broad peaks indicate the poor crystallinity of the α-Co(OH)<sub>2</sub> sample, which is beneficial for electrocatalytic processes. The amorphous materials may show superior activity over the corresponding crystalline forms for electrochemical applications due to the disordered structure. It has been reported that the amorphous Co(OH)<sub>2</sub> nanostructures exhibit outstanding capacitive performance and OER activity.<sup>87,91</sup> Furthermore, it has been reported that the virtual electrocatalyst for OER is the surface catalytically active layer composed of amorphous CoO<sub>x</sub>(OH)<sub>y</sub>, instead of the inner crystalline Co<sub>3</sub>O<sub>4</sub> in a recent work.<sup>92</sup> Thus, we consider that the amorphous characteristic of α-Co(OH)<sub>2</sub> can be responsible for the excellent OER performance in this work, which is due to defects, unordered structures, and anisotropy of amorphous materials. As can be seen from the magnified plot in Fig. 2(b), the peaks at 33.27° and 59.44° can be observed, which are consistent with α-Co(OH)<sub>2</sub>. All the diffraction peaks of another contrast sample are highly consistent with β-Co(OH)<sub>2</sub> (JCPDS: 74-1057).<sup>93</sup>

Generally, XPS is considered as a credible method to study the chemical states and coordination environment information of atoms in the material surfaces. In this study, to determine the surface oxidation states of the as-obtained α-Co(OH)<sub>2</sub> sample, an XPS survey was carried out and displayed in Fig. 3. In the Co 2p spectrum [Fig. 3(a)], the peaks of 2p<sub>3/2</sub> and 2p<sub>1/2</sub>, due to the spin–orbit coupling, are located at a binding energy of 780.7 and 796.4 eV with the shake-up satellites of the Co<sup>II</sup>,

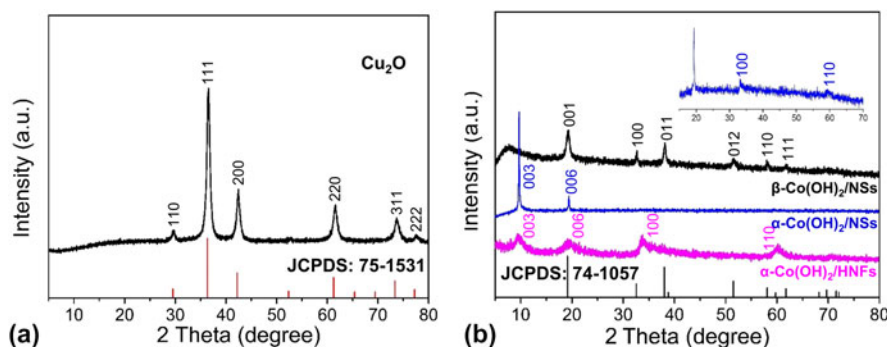


FIG. 2. XRD patterns of Cu<sub>2</sub>O templates (a) and α-Co(OH)<sub>2</sub>/HNFs, α-Co(OH)<sub>2</sub>/NSs, and β-Co(OH)<sub>2</sub>/NSs (b).

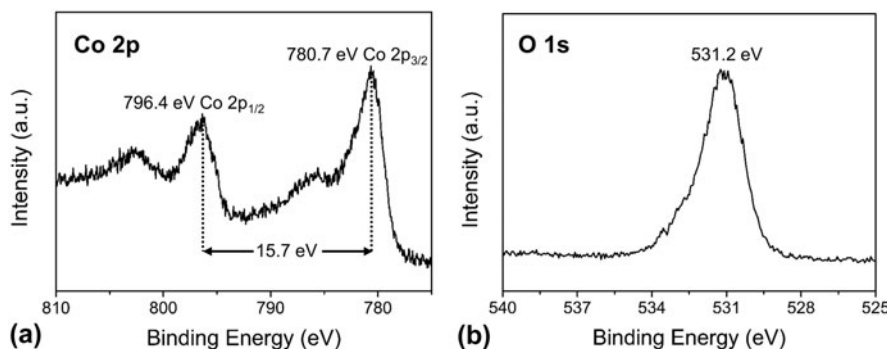


FIG. 3. XPS spectra of the α-Co(OH)<sub>2</sub>/HNFs: (a) Co 2p spectrum and (b) O 1s spectrum.

respectively. This is ascribed to the Co<sup>II</sup> oxidation state in Co(OH)<sub>2</sub>.<sup>94</sup> The corresponding shake-up satellite bands owing to plasmon losses and multielectron excitation appear in the higher binding energy region, further indicating the Co<sup>II</sup> oxidation state in the as-obtained α-Co(OH)<sub>2</sub> material. Generally, not only the general photoelectron lines but also satellite lines appear in the XPS spectrum of the latter 3d transition metal complex. As for the cobalt compound, Co<sup>II</sup> is distinguished from Co<sup>III</sup> due to the shake-up satellites for Co<sup>II</sup> but due to very weak or missing satellites for Co<sup>III</sup>. In addition, the spin-orbit splitting value of 2p<sub>1/2</sub> and 2p<sub>3/2</sub> is 15.7 eV, which is consistent with that in Co(OH)<sub>2</sub>.<sup>95</sup> In the O 1s spectrum [Fig. 3(b)], a single component locates at 531.2 eV corresponding to the oxygen in hydroxides as reported.

The porous structure and the specific surface area are always regarded as key factors beneficial for excellent electrocatalytic activity. The N<sub>2</sub> adsorption–desorption isotherms of the α-Co(OH)<sub>2</sub>/HNFs is shown in Fig. 4(a). The surface area of the α-Co(OH)<sub>2</sub>/HNFs is calculated as high as 78.13 m<sup>2</sup>/g by the Brunauer–Emmett–Teller (BET) method. The high surface area is originated from the self assembly of ultrathin nanosheets and well-formed hollow structures. The high surface area offers superior surface sites for OER. Figure 4(b) displays the pore size distribution of α-Co(OH)<sub>2</sub>/HNFs with the main pore diameter between 20 and 130 nm. Generally, polyporous materials possess excellent electrochemical activity due

to the exposure of active sites. Moreover, if the pore diameters are abundant, the corresponding polyporous materials will have superior OER performance owing to the quick mass diffusion. The experimental result from N<sub>2</sub> adsorption–desorption isotherms confirms the structural feature of α-Co(OH)<sub>2</sub> hollow nanoflowers.

## B. Electrocatalytic performance

The electrocatalytic OER performance of α-Co(OH)<sub>2</sub> hollow nanoflowers and contrast samples were evaluated by CV measurements in 1 M KOH solutions using a traditional three-electrode system. Figure 5(a) presents the CV curves of α-Co(OH)<sub>2</sub>/HNFs, α-Co(OH)<sub>2</sub>/NSs, and β-Co(OH)<sub>2</sub>/NSs. The overpotential is a crucial parameter for estimating the electrocatalytic water oxidation activity of the materials. As for α-Co(OH)<sub>2</sub>/HNFs, a current density of 10 mA/cm<sup>2</sup> was achieved at an overpotential of 310 mV, which is lower than the values of 324 and 360 mV required for Co(OH)<sub>2</sub>/NSs and β-Co(OH)<sub>2</sub>/NSs, respectively. The excellent OER activity of α-Co(OH)<sub>2</sub> hollow nanoflowers results from the following reasons. Generally speaking, the distinctive structure and amorphous characteristic of α-Co(OH)<sub>2</sub>/HNFs influence the electrochemical activity. Firstly, the unique hollow structure affords large spaces that are beneficial for fast diffusion of the electrolyte and releasing of gases. Beyond that, the outer ultrathin

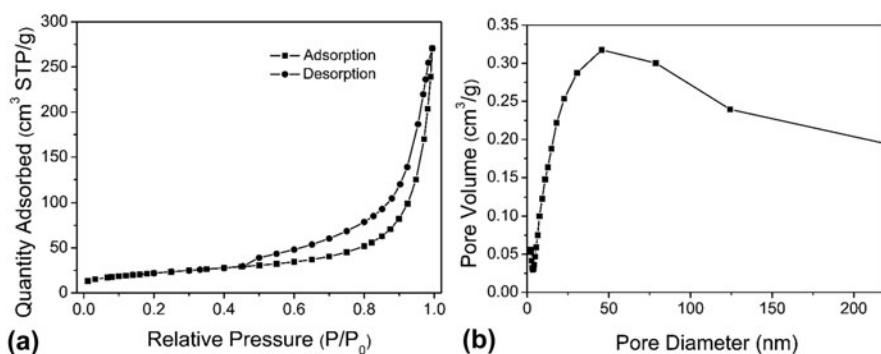


FIG. 4. (a) N<sub>2</sub> adsorption/desorption isotherms and (b) pore size distribution of  $\alpha$ -Co(OH)<sub>2</sub>/HNFs.

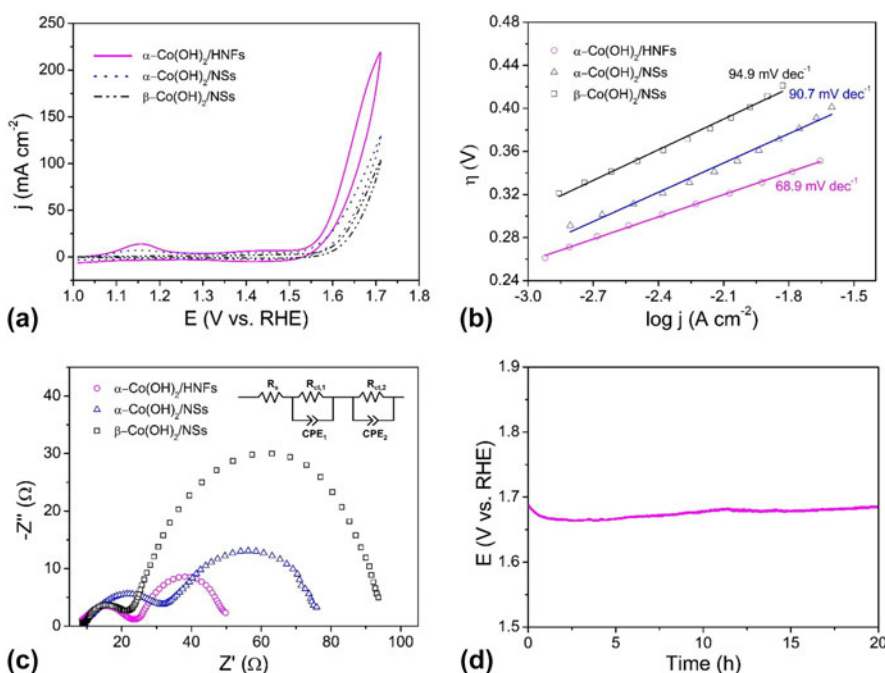


FIG. 5. (a) CV curves of  $\alpha$ -Co(OH)<sub>2</sub>/HNFs,  $\alpha$ -Co(OH)<sub>2</sub>/NSs and  $\beta$ -Co(OH)<sub>2</sub>/NSs in 1 M KOH; (b) Tafel plots for  $\alpha$ -Co(OH)<sub>2</sub>/HNFs,  $\alpha$ -Co(OH)<sub>2</sub>/NSs and  $\beta$ -Co(OH)<sub>2</sub>/NSs at scan rate of 1 mV/s; (c) EIS spectra of  $\alpha$ -Co(OH)<sub>2</sub>/HNFs,  $\alpha$ -Co(OH)<sub>2</sub>/NSs, and  $\beta$ -Co(OH)<sub>2</sub>/NSs. The inset is the equivalent circuit; (d) Chronopotentiometry curves at constant current density of 10 mA/cm<sup>2</sup> for the  $\alpha$ -Co(OH)<sub>2</sub>/HNFs without iR compensation with an ITO working electrode.

nanoflakes offer larger surface areas and more active sites giving rise to a high electrochemical OER activity. In other words, the superior surface areas from the unique hollow architecture and outer ultrathin nanoflakes play a significant role on the excellent activity. Secondly, the surfaces of  $\alpha$ -Co(OH)<sub>2</sub>/HNFs are three-dimensional due to the vertical ultrathin nanoflakes, which are more favorable to adsorb electrolytic ions in a reaction system than that of smooth nanospheres. Furthermore, a disordered structure and amorphous characteristic of the  $\alpha$ -Co(OH)<sub>2</sub> make contributions to the high performance. As mentioned above, the amorphous CoO<sub>x</sub>(OH)<sub>y</sub> surface layer rather than inner crystalline Co<sub>3</sub>O<sub>4</sub> made the main contribution to the

outstanding activity in other work. Thus, the amorphous characteristic of  $\alpha$ -Co(OH)<sub>2</sub>/HNFs bulk will account for the superior performance. Last, the porous structure resulted from hollow characteristic also be significant for the large surface areas, which further increase active sites. Additionally, the Tafel analytical method has been commonly used in the research of the OER process because reliable mechanistic and dynamics information can be obtained from the Tafel plot. The Tafel study gives the vital parameters of overpotential and exchange current density. Normally, high exchange current density is of equal importance with a low Tafel slope during the whole OER process.<sup>96</sup> As shown in Fig. 5(b), the corresponding Tafel plots demonstrate that the Tafel

slope of  $\alpha$ -Co(OH)<sub>2</sub>/HNFs is 68.9 mV/dec, which indicates a fast mass and electron transfer process. This value is much smaller than that of  $\alpha$ -Co(OH)<sub>2</sub>/NSs (90.7 mV/dec) and  $\beta$ -Co(OH)<sub>2</sub>/NSs (94.9 mV/dec).

To investigate electrode surface properties and reaction kinetics, EIS was carried out. Figure 5(c) displays the Nyquist plots of three catalysts, the first semicircle represents solution resistance including the resistance of the electrode material, electrolyte from the working electrode to the counter electrode and other possible resistance,<sup>97</sup> which is independent of the potential.<sup>32</sup> The OER efficiency can be evaluated by the second semicircle, which corresponds to the resistance of the charge transfer during the redox reactions. Generally, a smaller semicircle equals to a lower resistance value, which means a faster charge transfer rate. As shown in Fig. 5(c),  $\alpha$ -Co(OH)<sub>2</sub>/HNFs possesses the lowest resistance during OER due to the distinctive structural features, which suggest a quicker oxygen evolution rate of  $\alpha$ -Co(OH)<sub>2</sub>/HNFs than that of  $\alpha$ -Co(OH)<sub>2</sub>/NSs and  $\beta$ -Co(OH)<sub>2</sub>/NSs. The equivalent circuit was displayed, in which  $R_s$  represents the solution resistance,  $R_{ct}$  means the charge-transfer resistance, and CPE is a constant-phase element. Stability is another critical index for evaluating electrocatalysts especially for large-scale commercial applications. The long-term stability of Co(OH)<sub>2</sub>/HNFs was carried out by chronopotentiometry at a current density of 10 mA/cm<sup>2</sup> to maintain a constant potential of  $\sim$ 1.69 V for 20 h [Fig. 5(d)], which indicates that the as-prepared material is highly durable in an alkaline environment. Noteworthy, the unsmooth trace resulted from the formation of oxygen bubbles, which diffuse from the surface of the electrode to the electrolyte. Moreover, the required overpotential to realize a current density of 10 mA/cm<sup>2</sup> during the electrolysis was higher than that in the CV experiments. The higher overpotential in the electrolysis is reasonable with the following interpretations. On the one hand, CV studies were carried out with iR compensation, which was absent during electrolysis. On the other hand, an ITO electrode was introduced during electrolysis for

convenient O<sub>2</sub> release. However, slower mass transfer restricts the whole reaction, leading to higher overpotential for electrolysis. For the same reason, the current density in Fig. 5(d) is lower than that in Fig. 5(a) at the same potential, which is due to the absence of iR compensation during electrolysis. Of course, the lower current density was also caused by the slower mass transfer due to ITO working electrode with higher surface area used in electrolysis.

The ECSAs of the Co(OH)<sub>2</sub>/HNFs and the counterparts were obtained through investigating the double-layer capacitance ( $C_{dl}$ ) in the nonFaradaic potential region because the ECSA is in direct proportion to the  $C_{dl}$ . The calculation about ECSA is according to the following equations:

$$j_c = \nu C_{dl}/A \quad ,$$

$$ECSA = C_{dl}/C_s \quad ,$$

$j_c$  is the charging current density,  $\nu$  is the scan rate,  $C_{dl}$  is the double layer capacitance,  $A$  is the geometric area (0.07 cm<sup>2</sup>) of working electrode, and  $C_s$  is the specific capacitance value. Figure 6(a) shows the CV curves of Co(OH)<sub>2</sub>/HNFs with different scan rates at a potential window from 1.18 to 1.28 V versus RHE. Those of Co(OH)<sub>2</sub>/NSs and  $\beta$ -Co(OH)<sub>2</sub>/NSs can be seen in Fig. S2. As displayed in Fig. 6(b), the slope of the charging capacitive current versus the scan rate is equivalent to  $C_{dl}/A$ . The  $C_{dl}$  of Co(OH)<sub>2</sub>/HNFs is 2780  $\mu$ F through equations. Those of Co(OH)<sub>2</sub>/NSs and  $\beta$ -Co(OH)<sub>2</sub>/NSs are 1533  $\mu$ F and 861  $\mu$ F, respectively. Generally,  $C_s$  of Co-based materials is 27  $\mu$ F/cm<sup>2</sup> in 1 M KOH. Thus, the corresponding ECSAs are 103, 57, and 32 cm<sup>2</sup> for Co(OH)<sub>2</sub>/HNFs, Co(OH)<sub>2</sub>/NSs, and  $\beta$ -Co(OH)<sub>2</sub>/NSs in proper order. This result reveals that Co(OH)<sub>2</sub>/HNFs possesses the highest active surface area, which is mainly attributed to the unique hollow architecture and outer ultrathin nanoflakes that are electrochemically accessible.<sup>98</sup>

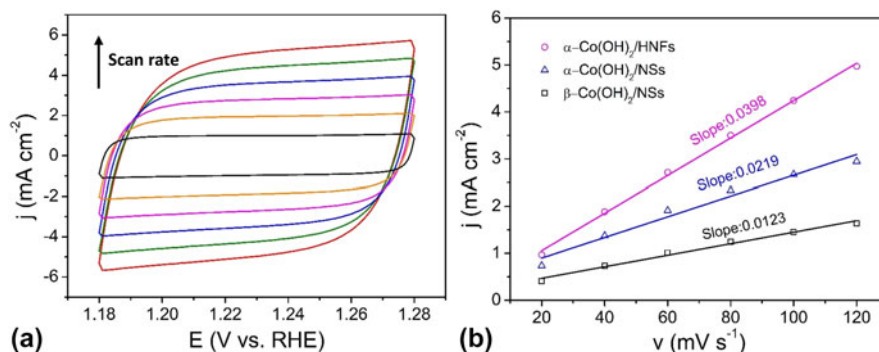


FIG. 6. (a) CV curves of the  $\alpha$ -Co(OH)<sub>2</sub>/HNFs in 1 M KOH at different scan rates from 20 to 120 mV/s; (b) Charging current densities at 1.23 V versus RHE plotted against the scan rate. The linear slope (equivalent to the  $C_{dl}$ ) was used to represent the ECSA.

## IV. CONCLUSIONS

In summary, we used a simple and highly efficient template-based method to synthesize amorphous  $\alpha$ -Co(OH)<sub>2</sub>/HNFs as highly active electrocatalysts for water oxidation in an alkaline solution. Moreover, the template-based method is superior to other traditional template synthesis because no other etching agents are used to remove the templates. Na<sub>2</sub>S<sub>2</sub>O<sub>3</sub> played roles as the alkali source and etching agent at the same time. Hard and soft acids and bases principle offers the theoretical basis for the choice of reaction reagent and solvent. The whole synthetic was accomplished under mild conditions. The 3D hollow nanoflower architecture, amorphous phase characteristic, surface information, and porous structure were expressed through a series of physical characterizations. The  $\alpha$ -Co(OH)<sub>2</sub>/HNFs exhibited a low overpotential of 310 mV at a current density of 10 mA/cm<sup>2</sup>, a low Tafel slope of 68.9 mV/dec, and at high electrochemical surface areas. Furthermore, the  $\alpha$ -Co(OH)<sub>2</sub>/HNFs displayed excellent durability for OER in 1 M KOH solution. The long-term chronopotentiometry at a current density of 10 mA/cm<sup>2</sup> can provide evidence with a stable potential of ~1.69 V for 20 h. The oxygen evolution kinetics was revealed from Tafel and EIS techniques. Significantly, the remarkable performance of  $\alpha$ -Co(OH)<sub>2</sub>/HNFs can be attributed to the unique hollow structure that is beneficial for fast mass and electron transfer process and the ultrathin nanoflakes that provide larger surface areas and more catalytic active sites. Additionally, the amorphous characteristic of  $\alpha$ -Co(OH)<sub>2</sub>/HNFs also made a contribution to the outstanding catalytic activity due to the anisotropy, defect, and unordered structure. Therefore, this work provides researchers with a facile method to fabricate amorphous metal hydroxides or oxides with potential electrochemical applications.

## ACKNOWLEDGMENTS

This work was supported by the National Natural Science Foundation of China (21101170, 21503126, and 21573139), the Fundamental Research Funds for the Central Universities (GK201603037), the Starting Research Funds of Shaanxi Normal University, and the “Thousand Talents Program” of China.

## REFERENCES

- W. Zhang, W.Z. Lai, and R. Cao: Energy-related small molecule activation reactions: Oxygen reduction and hydrogen and oxygen evolution reactions catalyzed by porphyrin- and corrole-based systems. *Chem. Rev.* **117**, 3717 (2017).
- J.R. Ran, J. Zhang, J.G. Yu, M. Jaroniec, and S.Z. Qiao: Earth-abundant cocatalysts for semiconductor-based photocatalytic water splitting. *Chem. Soc. Rev.* **43**, 7787 (2014).
- D. Gust, T.A. Moore, and A.L. Moore: Solar fuels via artificial photosynthesis. *Acc. Chem. Res.* **42**, 1890 (2009).
- V. Balzani, A. Credi, and M. Venturi: Photochemical conversion of solar energy. *ChemSusChem* **1**, 26 (2008).
- C. Xie, Y.Y. Wang, K. Hu, L. Tao, X.B. Huang, J. Huo, and S.Y. Wang: In situ confined synthesis of molybdenum oxide decorated nickel-iron alloy nanosheets from MoO<sub>4</sub><sup>2-</sup> intercalated layered double hydroxides for the oxygen evolution reaction. *J. Mater. Chem. A* **5**, 87 (2017).
- Z.J. Liu, Z.H. Zhao, Y.Y. Wang, S. Dou, D.F. Yan, D.D. Liu, Z.H. Xia, and S.Y. Wang: In situ exfoliated, edge-rich, oxygen-functionalized graphene from carbon fibers for oxygen electrocatalysis. *Adv. Mater.* **29**, 1606207 (2017).
- Y. Tachibana, L. Vayssieres, and J.R. Durrant: Artificial photosynthesis for solar water-splitting. *Nat. Photonics* **6**, 511 (2012).
- J. Ohi: Hydrogen energy cycle: An overview. *J. Mater. Res.* **20**, 3180 (2005).
- C.G. Morales-Guio, L.A. Stern, and X.L. Hu: Nanostructured hydrotreating catalysts for electrochemical hydrogen evolution. *Chem. Soc. Rev.* **43**, 6555 (2014).
- Y.M. Shi and B. Zhang: Recent advances in transition metal phosphide nanomaterials: Synthesis and applications in hydrogen evolution reaction. *Chem. Soc. Rev.* **45**, 1529 (2016).
- R. Zhang, X.X. Wang, S.J. Yu, T. Wen, X.W. Zhu, F.X. Yang, X.N. Sun, X.K. Wang, and W.P. Hu: Ternary NiCo<sub>2</sub>P<sub>x</sub> nanowires as pH-universal electrocatalysts for highly efficient hydrogen evolution reaction. *Adv. Mater.* **29**, 1605502 (2017).
- J. Yin, Q.H. Fan, Y.X. Li, F.Y. Cheng, P.P. Zhou, P.X. Xi, and S.H. Sun: Ni-C-N nanosheets as catalyst for hydrogen evolution reaction. *J. Am. Chem. Soc.* **138**, 14546 (2016).
- L. An, L. Huang, P.P. Zhou, J. Yin, H.Y. Liu, and P.X. Xi: A self-standing high-performance hydrogen evolution electrode with nanostructured NiCo<sub>2</sub>O<sub>4</sub>/CuS heterostructures. *Adv. Funct. Mater.* **25**, 6814 (2015).
- M.X. Chen, J. Qi, W. Zhang, and R. Cao: Electrosynthesis of NiP<sub>x</sub> nanospheres for electrocatalytic hydrogen evolution from a neutral aqueous solution. *Chem. Commun.* **53**, 5507 (2017).
- H.T. Lei, H.Y. Fang, Y.Z. Han, W.Z. Lai, X.F. Fu, and R. Cao: Reactivity and mechanism studies of hydrogen evolution catalyzed by copper corroles. *ACS Catal.* **5**, 5145 (2015).
- Y.Z. Han, H.Y. Fang, H.Z. Jing, H.L. Sun, H.T. Lei, W.Z. Lai, and R. Cao: Singly versus doubly reduced nickel porphyrins for proton reduction: Experimental and theoretical evidence for a homolytic hydrogen-evolution reaction. *Angew. Chem., Int. Ed.* **55**, 5457 (2016).
- M.G. Walter, E.L. Warren, J.R. McKone, S.W. Boettcher, Q. Mi, E.A. Santori, and N.S. Lewis: Solar water splitting cells. *Chem. Rev.* **110**, 6446 (2010).
- D.Y. Guo, J. Qi, W. Zhang, and R. Cao: Surface electrochemical modification of a nickel substrate to prepare a NiFe-based electrode for water oxidation. *ChemSusChem* **10**, 394 (2017).
- S.-C. Lin, Y.-F. Chiu, P.-W. Wu, Y.-F. Hsieh, and C.-Y. Wu: Templated fabrication of nanostructured Ni brush for hydrogen evolution reaction. *J. Mater. Res.* **25**, 2001 (2010).
- S.H. Shen: Toward efficient solar water splitting over hematite photoelectrodes. *J. Mater. Res.* **29**, 29 (2013).
- Y. Zhang, Y. Xie, Y.T. Zhou, X.W. Wang, and K. Pan: Well dispersed Fe<sub>2</sub>N nanoparticles on surface of nitrogen-doped reduced graphite oxide for highly efficient electrochemical hydrogen evolution. *J. Mater. Res.* **32**, 1770 (2017).
- C.J. Gagliardi, B.C. Westlake, C.A. Kent, J.J. Paul, J.M. Papanikolas, and T.J. Meyer: Integrating proton coupled electron transfer (PCET) and excited states. *Coord. Chem. Rev.* **254**, 2459 (2010).
- M.X. Chen, Y.Z. Wu, Y.Z. Han, X.H. Lin, J.L. Sun, W. Zhang, and R. Cao: An iron-based film for highly efficient electrocatalytic oxygen evolution from neutral aqueous solution. *ACS Appl. Mater. Interfaces* **7**, 21852 (2015).

24. R. Cao, W.Z. Lai, and P.W. Du: Catalytic water oxidation at single metal sites. *Energy Environ. Sci.* **5**, 8134 (2012).
25. Y.Z. Wu, M.X. Chen, Y.Z. Han, H.X. Luo, X.J. Su, M.T. Zhang, X.H. Lin, J.L. Sun, L. Wang, L. Deng, W. Zhang, and R. Cao: Fast and simple preparation of iron-based thin films as highly efficient water-oxidation catalysts in neutral aqueous solution. *Angew. Chem., Int. Ed.* **54**, 4870 (2015).
26. T.R. Cook, D.K. Dogutan, S.Y. Reece, Y. Surendranath, T.S. Teets, and D.G. Nocera: Solar energy supply and storage for the legacy and nonlegacy worlds. *Chem. Rev.* **110**, 6474 (2010).
27. Y. Lee, J. Suntivich, K.J. May, E.E. Perry, and Y. Shao-Horn: Synthesis and activities of rutile IrO<sub>2</sub> and RuO<sub>2</sub> nanoparticles for oxygen evolution in acid and alkaline solutions. *J. Phys. Chem. Lett.* **3**, 399 (2012).
28. D.F. Yan, Y.X. Li, J. Huo, R. Chen, L.M. Dai, and S.Y. Wang: Defect chemistry of nonprecious-metal electrocatalysts for oxygen reactions. *Adv. Mater.* **29**, 1606459 (2017).
29. S. Chen and S.Z. Qiao: Hierarchically porous nitrogen-doped graphene–NiCo<sub>2</sub>O<sub>4</sub> hybrid paper as an advanced electrocatalytic water-splitting material. *ACS Nano* **7**, 10190 (2013).
30. G.S. Hutchings, Y. Zhang, J. Li, B.T. Yonemoto, X.G. Zhou, K.K. Zhu, and F. Jiao: In situ formation of cobalt oxide nanocubanes as efficient oxygen evolution catalysts. *J. Am. Chem. Soc.* **137**, 4223 (2015).
31. J. Kim, J.S. Kim, H. Baik, K. Kang, and K. Lee: Porous β-MnO<sub>2</sub> nanoplates derived from MnCO<sub>3</sub> nanoplates as highly efficient electrocatalysts toward oxygen evolution reaction. *RSC Adv.* **6**, 26535 (2016).
32. J. Qi, W. Zhang, R.J. Xiang, K.Q. Liu, H.Y. Wang, M.X. Chen, Y.Z. Han, and R. Cao: Porous nickel-iron oxide as a highly efficient electrocatalyst for oxygen evolution reaction. *Adv. Sci.* **2**, 1500199 (2015).
33. C.H. Kuo, I.M. Mosa, A.S. Poyraz, S. Biswas, A.M. E-Sawy, W.Q. Song, Z. Luo, S.Y. Chen, J.F. Rusling, J. He, and S.L. Suib: Robust mesoporous manganese oxide catalysts for water oxidation. *ACS Catal.* **5**, 1693 (2015).
34. K. Fominykh, J.M. Feckl, J. Sicklinger, M. Doblinger, S. Bocklein, J. Ziegler, L. Peter, J. Rathousky, E.W. Scheidt, T. Bein, and D. Fattakhova-Rohlfing: Ultrasmall dispersible crystalline nickel oxide nanoparticles as high-performance catalysts for electrochemical water splitting. *Adv. Funct. Mater.* **24**, 3123 (2014).
35. R.D. Smith, M.S. Prevot, R.D. Fagan, S. Trudel, and C.P. Berlinguette: Water oxidation catalysis: Electrocatalytic response to metal stoichiometry in amorphous metal oxide films containing iron, cobalt, and nickel. *J. Am. Chem. Soc.* **135**, 11580 (2013).
36. L. Kuai, J. Geng, C.Y. Chen, E.J. Kan, Y.D. Liu, Q. Wang, and B.Y. Geng: A reliable aerosol-spray-assisted approach to produce and optimize amorphous metal oxide catalysts for electrochemical water splitting. *Angew. Chem., Int. Ed.* **53**, 7547 (2014).
37. H.T. Wang, H.W. Lee, Y. Deng, Z.Y. Lu, P.C. Hsu, Y.Y. Liu, D.C. Lin, and Y. Cui: Bifunctional non-noble metal oxide nanoparticle electrocatalysts through lithium-induced conversion for overall water splitting. *Nat. Commun.* **6**, 7261 (2015).
38. S. Jung, C.C.L. McCrory, I.M. Ferrer, J.C. Peters, and T.F. Jaramillo: Benchmarking nanoparticulate metal oxide electrocatalysts for the alkaline water oxidation reaction. *J. Mater. Chem. A* **4**, 3068 (2016).
39. G.Q. Han, Y.R. Liu, W.H. Hu, B. Dong, X. Li, X. Shang, Y.M. Chai, Y.Q. Liu, and C.G. Liu: Crystallographic structure and morphology transformation of MnO<sub>2</sub> nanorods as efficient electrocatalysts for oxygen evolution reaction. *J. Electrochem. Soc.* **163**, H67 (2015).
40. W. Zhang, J. Qi, K.Q. Liu, and R. Cao: A nickel-based integrated electrode from an autologous growth strategy for highly efficient water oxidation. *Adv. Energy Mater.* **6**, 1502489 (2016).
41. W. Zhang, Y.Z. Wu, J. Qi, M.X. Chen, and R. Cao: A thin NiFe hydroxide film formed by stepwise electrodeposition strategy with significantly improved catalytic water oxidation efficiency. *Adv. Energy Mater.* **7**, 1602547 (2017).
42. M.R. Gao, W.C. Sheng, Z.B. Zhuang, Q.R. Fang, S. Gu, J. Jiang, and Y.S. Yan: Efficient water oxidation using nanostructured α-nickel-hydroxide as an electrocatalyst. *J. Am. Chem. Soc.* **136**, 7077 (2014).
43. M.W. Louie and A.T. Bell: An investigation of thin-film Ni–Fe oxide catalysts for the electrochemical evolution of oxygen. *J. Am. Chem. Soc.* **135**, 12329 (2013).
44. L. Trotochaud, S.L. Young, J.K. Ranney, and S.W. Boettcher: Nickel–iron oxyhydroxide oxygen-evolution electrocatalysts: The role of intentional and incidental iron incorporation. *J. Am. Chem. Soc.* **136**, 6744 (2014).
45. D. Friebe, M.W. Louie, M. Bajdich, K.E. Sanwald, Y. Cai, A.M. Wise, M.J. Cheng, D. Sokaras, T.C. Weng, R. Alonso-Mori, R.C. Davis, J.R. Bargar, J.K. Norskov, A. Nilsson, and A.T. Bell: Identification of highly active Fe sites in (Ni,Fe)OOH for electrocatalytic water splitting. *J. Am. Chem. Soc.* **137**, 1305 (2015).
46. P.F. Liu, S. Yang, B. Zhang, and H.G. Yang: Defect-rich ultrathin cobalt-iron layered double hydroxide for electrochemical overall water splitting. *ACS Appl. Mater. Interfaces* **8**, 34474 (2016).
47. F. Song and X.L. Hu: Ultrathin cobalt-manganese layered double hydroxide is an efficient oxygen evolution catalyst. *J. Am. Chem. Soc.* **136**, 16481 (2014).
48. Y. Zhang, B. Cui, C.S. Zhao, H. Lin, and J.B. Li: Co–Ni layered double hydroxides for water oxidation in neutral electrolyte. *Phys. Chem. Chem. Phys.* **15**, 7363 (2013).
49. C. Zhang, M.F. Shao, L. Zhou, Z.H. Li, K.M. Xiao, and M. Wei: Hierarchical NiFe layered double hydroxide hollow microspheres with highly-efficient behavior toward oxygen evolution reaction. *ACS Appl. Mater. Interfaces* **8**, 33697 (2016).
50. Y.Y. Wang, Y.Q. Zhang, Z.J. Liu, C. Xie, S. Feng, D.D. Liu, M.F. Shao, and S.Y. Wang: Layered double hydroxide nanosheets with multiple vacancies obtained by dry exfoliation as highly efficient oxygen evolution electrocatalysts. *Angew. Chem., Int. Ed.* **56**, 5867 (2017).
51. R. Liu, Y.Y. Wang, D.D. Liu, Y.Q. Zou, and S.Y. Wang: Water-plasma-enabled exfoliation of ultrathin layered double hydroxide nanosheets with multivacancies for water oxidation. *Adv. Mater.* **29**, 1701546 (2017).
52. J. Zhang, T. Wang, D. Pohl, B. Rellinghaus, R.H. Dong, S.H. Liu, X.D. Zhuang, and X.L. Feng: Interface engineering of MoS<sub>2</sub>/Ni<sub>3</sub>S<sub>2</sub> heterostructures for highly enhanced electrochemical overall-water-splitting activity. *Angew. Chem., Int. Ed.* **55**, 6702 (2016).
53. G.F. Chen, T.Y. Ma, Z.Q. Liu, N. Li, Y.Z. Su, K. Davey, and S.Z. Qiao: Efficient and stable bifunctional electrocatalysts Ni/Ni<sub>3</sub>M<sub>2</sub> (M = P, S) for overall water splitting. *Adv. Funct. Mater.* **26**, 3314 (2016).
54. T.T. Liu, Y.H. Liang, Q. Liu, X.P. Sun, Y.Q. He, and A.M. Asiri: Electrodeposition of cobalt–sulfide nanosheets film as an efficient electrocatalyst for oxygen evolution reaction. *Electrochem. Commun.* **60**, 92 (2015).
55. W.J. Zhou, X.J. Wu, X.H. Cao, X. Huang, C.L. Tan, J. Tian, H. Liu, J.Y. Wang, and H. Zhang: Ni<sub>3</sub>S<sub>2</sub> nanorods/Ni foam composite electrode with low overpotential for electrocatalytic oxygen evolution. *Energy Environ. Sci.* **6**, 2921 (2013).
56. Z. Gao, J. Qi, M.X. Chen, W. Zhang, and R. Cao: An electrodeposited NiSe for electrocatalytic hydrogen and oxygen evolution reactions in alkaline solution. *Electrochim. Acta* **224**, 412 (2017).

57. D.S. Kong, H.T. Wang, Z.Y. Lu, and Y. Cui: CoSe<sub>2</sub> nanoparticles grown on carbon fiber paper: An efficient and stable electrocatalyst for hydrogen evolution reaction. *J. Am. Chem. Soc.* **136**, 4897 (2014).
58. A.T. Swesi, J. Masud, and M. Nath: Enhancing electrocatalytic activity of bifunctional Ni<sub>3</sub>Se<sub>2</sub> for overall water splitting through etching-induced surface nanostructuring. *J. Mater. Res.* **31**, 2888 (2016).
59. Y.W. Liu, H. Cheng, M.J. Lyu, S.J. Fan, Q.H. Liu, W.S. Zhang, Y.D. Zhi, C.M. Wang, C. Xiao, S.Q. Wei, B.J. Ye, and Y. Xie: Low overpotential in vacancy-rich ultrathin CoSe<sub>2</sub> nanosheets for water oxidation. *J. Am. Chem. Soc.* **136**, 15670 (2014).
60. R. Xu, R. Wu, Y.M. Shi, J.F. Zhang, and B. Zhang: Ni<sub>3</sub>Se<sub>2</sub> nanoforest/Ni foam as a hydrophilic, metallic, and self-supported bifunctional electrocatalyst for both H<sub>2</sub> and O<sub>2</sub> generations. *Nano Energy* **24**, 103 (2016).
61. C. Tang, N.Y. Cheng, Z.H. Pu, W. Xing, and X.P. Sun: NiSe nanowire film supported on nickel foam: An efficient and stable 3D bifunctional electrode for full water splitting. *Angew. Chem., Int. Ed.* **54**, 9351 (2015).
62. A.J. Esswein, Y. Surendranath, S.Y. Reece, and D.G. Nocera: Highly active cobalt phosphate and borate based oxygen evolving catalysts operating in neutral and natural waters. *Energy Environ. Sci.* **4**, 499 (2011).
63. J. Masa, P. Weide, D. Peeters, I. Sinev, W. Xia, Z.Y. Sun, C. Somsen, M. Muhler, and W. Schuhmann: Amorphous cobalt boride (Co<sub>2</sub>B) as a highly efficient nonprecious catalyst for electrochemical water splitting: Oxygen and hydrogen evolution. *Adv. Energy Mater.* **6**, 1502313 (2016).
64. Y.J. Tang, C.H. Liu, W. Huang, X.L. Wang, L.Z. Dong, S.L. Li, and Y.Q. Lan: Bimetallic carbides-based nanocomposite as superior electrocatalyst for oxygen evolution reaction. *ACS Appl. Mater. Interfaces* **9**, 16977 (2017).
65. P.Z. Chen, K. Xu, Z.W. Fang, Y. Tong, J.C. Wu, X.L. Lu, X. Peng, H. Ding, C.Z. Wu, and Y. Xie: Metallic Co<sub>4</sub>N porous nanowire arrays activated by surface oxidation as electrocatalysts for the oxygen evolution reaction. *Angew. Chem., Int. Ed.* **54**, 14710 (2015).
66. K. Xu, P.Z. Chen, X.L. Li, Y. Tong, H. Ding, X.J. Wu, W.S. Chu, Z.M. Peng, C.Z. Wu, and Y. Xie: Metallic nickel nitride nanosheets realizing enhanced electrochemical water oxidation. *J. Am. Chem. Soc.* **137**, 4119 (2015).
67. D. Li, H. Baydoun, B. Kulikowski, and S.L. Brock: Boosting the catalytic performance of iron phosphide nanorods for the oxygen evolution reaction by incorporation of manganese. *Chem. Mater.* **29**, 3048 (2017).
68. M.J. Liu and J.H. Li: Cobalt phosphide hollow polyhedron as efficient bifunctional electrocatalysts for the evolution reaction of hydrogen and oxygen. *ACS Appl. Mater. Interfaces* **8**, 2158 (2016).
69. C.G. Read, J.F. Callejas, C.F. Holder, and R.E. Schaak: General strategy for the synthesis of transition metal phosphide films for electrocatalytic hydrogen and oxygen evolution. *ACS Appl. Mater. Interfaces* **8**, 12798 (2016).
70. S.T. Wei, K. Qi, Z. Jin, J.S. Cao, W.T. Zheng, H. Chen, and X.Q. Cui: One-step synthesis of a self-supported copper phosphide nanobush for overall water splitting. *ACS Omega* **1**, 1367 (2016).
71. X.G. Wang, W. Li, D.H. Xiong, and L.F. Liu: Fast fabrication of self-supported porous nickel phosphide foam for efficient, durable oxygen evolution and overall water splitting. *J. Mater. Chem. A* **4**, 5639 (2016).
72. X.Y. Yu, Y. Feng, B.Y. Guan, X.W. Lou, and U. Paik: Carbon coated porous nickel phosphides nanoplates for highly efficient oxygen evolution reaction. *Energy Environ. Sci.* **9**, 1246 (2016).
73. E.J. Popczun, J.R. McKone, C.G. Read, A.J. Biccchi, A.M. Wiltrout, N.S. Lewis, and R.E. Schaak: Nanostructured nickel phosphide as an electrocatalyst for the hydrogen evolution reaction. *J. Am. Chem. Soc.* **135**, 9267 (2013).
74. D. Li, H. Baydoun, C.N. Verani, and S.L. Brock: Efficient water oxidation using CoMnP nanoparticles. *J. Am. Chem. Soc.* **138**, 4006 (2016).
75. G. Zhang, G.C. Wang, Y. Liu, H.J. Liu, J.H. Qu, and J.H. Li: Highly active and stable catalysts of phytic acid-derivative transition metal phosphides for full water splitting. *J. Am. Chem. Soc.* **138**, 14686 (2016).
76. M. Ledendecker, S. Krick Calderon, C. Papp, H.P. Steinruck, M. Antonietti, and M. Shalom: The synthesis of nanostructured Ni<sub>5</sub>P<sub>4</sub> films and their use as a non-noble bifunctional electrocatalyst for full water splitting. *Angew. Chem., Int. Ed.* **54**, 12361 (2015).
77. W.Z. Lai, R. Cao, G. Dong, S. Shaik, J.N. Yao, and H. Chen: Why is cobalt the best transition metal in transition-metal handman corroles for O–O bond formation during water oxidation? *J. Phys. Chem. Lett.* **3**, 2315 (2012).
78. V. Artero, M. Chavarot-Kerlidou, and M. Fontecave: Splitting water with cobalt. *Angew. Chem., Int. Ed.* **50**, 7238 (2011).
79. S.H. Wan, J. Qi, W. Zhang, W.N. Wang, S.K. Zhang, K.Q. Liu, H.Q. Zheng, J.L. Sun, S.Y. Wang, and R. Cao: Hierarchical Co(OH)F superstructure built by low-dimensional substructures for electrocatalytic water oxidation. *Adv. Mater.* **29**, 1700286 (2017).
80. D.Y. Guo, F.F. Chen, W. Zhang, and R. Cao: Phase-transfer synthesis of  $\alpha$ -Co(OH)<sub>2</sub> and its conversion to CoO for efficient electrocatalytic water oxidation. *Sci. Bull.* **62**, 626 (2017).
81. J.H. Wang, W. Cui, Q. Liu, Z.C. Xing, A.M. Asiri, and X.P. Sun: Recent progress in cobalt-based heterogeneous catalysts for electrochemical water splitting. *Adv. Mater.* **28**, 215 (2016).
82. S. Dou, C.L. Dong, Z. Hu, Y.C. Huang, J.I. Chen, L. Tao, D.F. Yan, D.W. Chen, S.H. Shen, S.L. Chou, and S.Y. Wang: Atomic-scale CoO<sub>x</sub> species in metal-organic frameworks for oxygen evolution reaction. *Adv. Funct. Mater.* **27**, 1702546 (2017).
83. R.M. Liu, Z.X. Jiang, J.P. Ma, L. Ni, X.Y. Sun, Y. Liu, H.X. Chen, and Q. Liu: Al<sup>3+</sup>-induced growth of  $\alpha$ -Co(OH)<sub>2</sub> nanoplates as high-capacity supercapacitors and water oxidation electrocatalysts. *RSC Adv.* **7**, 3783 (2017).
84. L. Wang, Z.H. Dong, Z.G. Wang, F.X. Zhang, and J. Jin: Layered  $\alpha$ -Co(OH)<sub>2</sub> nanocones as electrode materials for pseudocapacitors: Understanding the effect of interlayer space on electrochemical activity. *Adv. Funct. Mater.* **23**, 2758 (2013).
85. Y.M. Jiang, X. Li, T.X. Wang, and C.M. Wang: Enhanced electrocatalytic oxygen evolution of  $\alpha$ -Co(OH)<sub>2</sub> nanosheets on carbon nanotube/polyimide films. *Nanoscale* **8**, 9667 (2016).
86. P.F. Liu, S. Yang, L.R. Zheng, B. Zhang, and H.G. Yang: Electrochemical etching of  $\alpha$ -cobalt hydroxide for improvement of oxygen evolution reaction. *J. Mater. Chem. A* **4**, 9578 (2016).
87. M.A. Sayeed, T. Herd, and A.P. O'Mullane: Direct electrochemical formation of nanostructured amorphous Co(OH)<sub>2</sub> on gold electrodes with enhanced activity for the oxygen evolution reaction. *J. Mater. Chem. A* **4**, 991 (2016).
88. J.T. Zhang, J.F. Liu, Q. Peng, X. Wang, and Y.D. Li: Nearly monodisperse Cu<sub>2</sub>O and CuO nanospheres: Preparation and applications for sensitive gas sensors. *Chem. Mater.* **18**, 867 (2006).
89. J.W. Nai, Y. Tian, X. Guan, and L. Guo: Pearson's principle inspired generalized strategy for the fabrication of metal hydroxide and oxide nanocages. *J. Am. Chem. Soc.* **135**, 16082 (2013).
90. Y.P. Zhu, T.Y. Ma, M. Jaroniec, and S.Z. Qiao: Self-templating synthesis of hollow Co<sub>3</sub>O<sub>4</sub> microtube arrays for highly efficient water electrolysis. *Angew. Chem., Int. Ed.* **56**, 1324 (2017).

91. H.B. Li, M.H. Yu, X.H. Lu, P. Liu, Y. Liang, J. Xiao, Y.X. Tong, and G.W. Yang: Amorphous cobalt hydroxide with superior pseudocapacitive performance. *ACS Appl. Mater. Interfaces* **6**, 745 (2014).
92. A. Bergmann, E. Martinez-Moreno, D. Teschner, P. Cherev, M. Gliech, J.F. de Araujo, T. Reier, H. Dau, and P. Strasser: Reversible amorphization and the catalytically active state of crystalline Co<sub>3</sub>O<sub>4</sub> during oxygen evolution. *Nat. Commun.* **6**, 8625 (2015).
93. Z.P. Liu, R.Z. Ma, M. Osada, K. Takada, and T. Sasaki: Selective and controlled synthesis of  $\alpha$ - and  $\beta$ -cobalt hydroxides in highly developed hexagonal platelets. *J. Am. Chem. Soc.* **127**, 13869 (2005).
94. J. Yang, H.W. Liu, W.N. Martens, and R.L. Frost: Synthesis and characterization of cobalt hydroxide, cobalt oxyhydroxide, and cobalt oxide nanodiscs. *J. Phys. Chem. C* **114**, 111 (2010).
95. T. Xue, X. Wang, and J.M. Lee: Dual-template synthesis of Co(OH)<sub>2</sub> with mesoporous nanowire structure and its application in supercapacitor. *J. Power Sources* **201**, 382 (2012).
96. Y.Q. Lai, Y. Li, L.X. Jiang, W. Xu, X.J. Lv, J. Li, and Y.X. Liu: Electrochemical behaviors of co-deposited Pb/Pb-MnO<sub>2</sub> composite anode in sulfuric acid solution—Tafel and EIS investigations. *J. Electroanal. Chem.* **671**, 16 (2012).
97. H.Y. Jin, S.J. Mao, G.P. Zhan, F. Xu, X.B. Bao, and Y. Wang: Fe incorporated  $\alpha$ -Co(OH)<sub>2</sub> nanosheets with remarkably improved activity towards the oxygen evolution reaction. *J. Mater. Chem. A* **5**, 1078 (2017).
98. F. Song and X.L. Hu: Exfoliation of layered double hydroxides for enhanced oxygen evolution catalysis. *Nat. Commun.* **5**, 4477 (2014).

### Supplementary Material

To view supplementary material for this article, please visit <https://doi.org/10.1557/jmr.2017.390>.